

WILEY-VCH



European Chemical  
Societies Publishing

# Take Advantage and Publish Open Access



By publishing your paper open access, you'll be making it immediately freely available to anyone everywhere in the world.

That's maximum access and visibility worldwide with the same rigor of peer review you would expect from any high-quality journal.

**Submit your paper today.**



[www.chemistry-europe.org](http://www.chemistry-europe.org)

# Brønsted Acid versus Phase-Transfer Catalysis in the Enantioselective Transannular Aminohalogenation of Enesultams

Javier Luis-Barrera,<sup>[a]</sup> Sandra Rodriguez,<sup>[a]</sup> Uxue Uria,<sup>\*,[a]</sup> Efraim Reyes,<sup>[a]</sup> Liher Prieto,<sup>[a]</sup> Luisa Carrillo,<sup>[a]</sup> Manuel Pedrón,<sup>[b]</sup> Tomás Tejero,<sup>[c]</sup> Pedro Merino,<sup>\*,[b]</sup> and Jose L. Vicario<sup>\*,[a]</sup>

**Abstract:** We have studied the enantioselective transannular aminohalogenation reaction of unsaturated medium-sized cyclic benzosulfonamides by using both chiral Brønsted acid and phase-transfer catalysis. Under optimized conditions, a variety of bicyclic adducts can be obtained with good yields and high enantioselectivities. The mechanism of the reaction

was also studied by using computational tools; we observed that the reaction involves the participation of a conformer of the nine-membered cyclic substrate with planar chirality in which the stereochemical outcome is controlled by the relative reactivity of the two pseudorotational enantiomers when interacting with the chiral catalyst.

## Introduction

Transannular reactions constitute a powerful yet significantly underdeveloped approach for the synthesis of relatively complex polycyclic scaffolds.<sup>[1]</sup> This type of reaction, in which the two reacting points are incorporated at nonadjacent positions within the structure of a medium or large sized cyclic compound, shows up as an unconventional method for the construction of a given target compound that typically benefit from the low degree of conformational freedom of the cyclic starting material. This situation very often conditions the structure of the final product, in many cases providing reactivity profiles that differ from the ones observed corresponding intermolecular reaction. Moreover, this fixed preferred geometry on the starting material also calls for a very favorable

situation for transannular reactions when stereocontrol is desired. In this context, the literature is rich in examples of highly diastereoselective transannular reactions that take place under substrate control when a chiral starting material is employed.<sup>[2]</sup> In contrast, the number of examples of enantioselective reactions that convert an achiral cyclic starting material into an enantioenriched polycyclic product is very scarce.<sup>[3]</sup> All these transformations consist on either pericyclic processes or make use of activated alkenes as the electrophile undergoing transannular reaction with an internal nucleophile incorporated at the starting material.

In a different approach, we wish to present herein our recent studies towards the development of a catalytic and enantioselective version of a transannular aminohalogenation process employing enebenzosultams as substrates in which a nonactivated alkene is employed as the internal electrophile undergoing the transannular process after activation by an electrophilic halogen source (Scheme 1).

[a] Dr. J. Luis-Barrera, Dr. S. Rodriguez, Dr. U. Uria, Dr. E. Reyes, Dr. L. Prieto, Prof. Dr. L. Carrillo, Prof. Dr. J. L. Vicario  
Department of Organic and Inorganic Chemistry  
University of the Basque Country (UPV/EHU)  
P.O. Box 644, 48080 Bilbao (Spain)  
E-mail: uxue.uria@ehu.es  
jose Luis.vicario@ehu.es

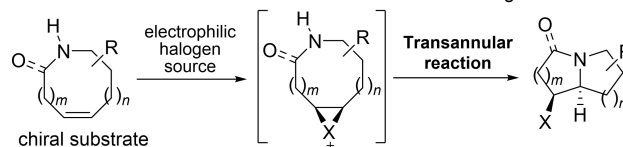
[b] M. Pedrón, Prof. Dr. P. Merino  
Instituto de Biocomputación y Física de Sistemas Complejos (BIFI)  
Universidad de Zaragoza  
50009 Zaragoza (Spain)  
E-mail: pmerino@unizar.es

[c] Prof. Dr. T. Tejero  
Instituto de Síntesis Química y Catálisis Homogénea (ISQCH)  
Universidad de Zaragoza-CSIC  
50009 Zaragoza (Spain)

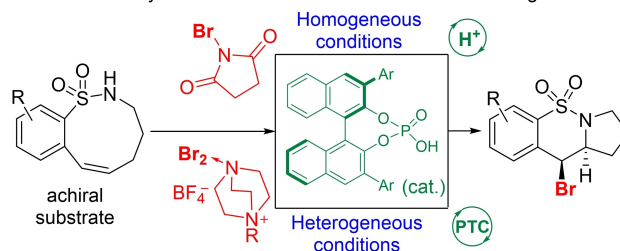
Supporting information for this article is available on the WWW under <https://doi.org/10.1002/chem.202202267>

Part of a Special Collection for the 8th EuChemS Chemistry Congress 2022 consisting of contributions from selected speakers and conveners. To view the complete collection, visit "[https://chemistry-europe.onlinelibrary.wiley.com/doi/toc/10.1002/\(ISSN\)1521-3765.8th-euchems\\_chem\\_congr/](https://chemistry-europe.onlinelibrary.wiley.com/doi/toc/10.1002/(ISSN)1521-3765.8th-euchems_chem_congr/)" 8th EuChemS Chemistry Congress.

**Previous work:** Diastereoselective transannular aminohalogenation



**This work:** Catalytic enantioselective transannular aminohalogenation



**Scheme 1.** Stereocontrolled transannular aminohalogenation reactions.

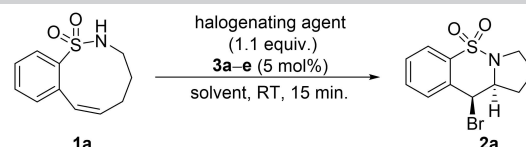
It should be pointed out that there are several examples of transannular aminohalogenation reactions described in the literature,<sup>[4]</sup> although, as mentioned earlier, all of them relying on the use of an enantioenriched chiral starting material and in which typically high diastereoselectivity is obtained by means of the asymmetric induction exerted by the stereogenic centers present at the substrates. In this sense, a catalytic and enantioselective version of a transannular aminohalogenation process is still elusive.

As is also shown in Scheme 1, the reaction design would involve the initial activation of the alkene moiety with a selected electrophilic halogen source in the presence of a chiral catalyst. Subsequently, the transannular process would undergo, being the stereochemistry of the overall process controlled by the presence of the chiral catalyst.<sup>[5]</sup> In this context, and among the different strategies described for catalytic enantioselective aminohalogenation reactions, we turned our attention to the possibility of using BINOL-based phosphoric acids as Brønsted acid catalyst for both the activation of the electrophilic halogen source and for achieving stereocontrol. Under this organocatalytic activation manifold, two different concepts have been applied to induce enantiocontrol: On one hand, a soluble halogenating reagent (such as NBS or related *N*-haloimide reagents) undergoes activation by the chiral Brønsted acid catalyst itself<sup>[6]</sup> or, on the other, an insoluble electrophilic halogen source is employed in the reaction, being the BINOL-based phosphoric acid involved as a chiral phase-transfer catalyst.<sup>[7]</sup> Both approaches will be evaluated in this reaction.

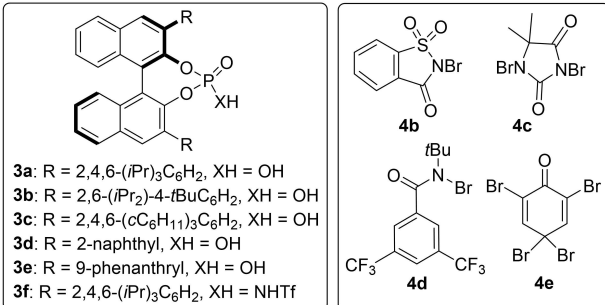
## Results and Discussion

We started by searching for the optimal reaction conditions that provide the compound **2a** with the best yield and enantioselectivity using enesultam **1a** as model system (Table 1). The initial reaction using NBS as halogenating agent and in the presence of the archetypical chiral phosphoric acid (*R*)-TRIP (**3a**) as catalyst provided the desired transannular aminobromination product **2a** in a promising 65% *ee* after 15 minutes (Table 1, entry 1). Remarkably, the reaction in the absence of acid catalyst under the same conditions was also effective, although it required a significantly longer reaction time (3 h, Table 1, entry 2). Other phosphoric acid catalysts **3b–f** were also evaluated but, even in all cases the reaction proceeded fast and furnished a high yield of **2a**, in all cases enantioselectivities were significantly lower to those provided by **3a** (Table 1, entries 3–7). Solvent effect was also evaluated, observing that moving to chloroform resulted into an important decrease in enantioselectivity (Table 1, entry 8), while the reaction performed similarly when moving from toluene to chlorobenzene (Table 1, entry 9 vs. 1). On the other hand, a slight improvement in the enantiocontrol was found working in *m*-xylene and in mesitylene (Table 1, entry 10 and 11). Other halogenating agents were tested (Table 1, entries 12–15) using mesitylene but none of them provided improved performance with respect to the results obtained with NBS, which was therefore selected as the optimal electrophilic bromine source.<sup>[8]</sup> We next carried

**Table 1.** Screening for the best reaction conditions.<sup>[a]</sup>



**3a:** R = 2,4,6-(*i*Pr)<sub>3</sub>C<sub>6</sub>H<sub>2</sub>, XH = OH  
**3b:** R = 2,6-(*i*Pr)<sub>2</sub>-4-*t*BuC<sub>6</sub>H<sub>2</sub>, XH = OH  
**3c:** R = 2,4,6-(*c*C<sub>6</sub>H<sub>11</sub>)<sub>3</sub>C<sub>6</sub>H<sub>2</sub>, XH = OH  
**3d:** R = 2-naphthyl, XH = OH  
**3e:** R = 9-phenanthryl, XH = OH  
**3f:** R = 2,4,6-(*i*Pr)<sub>3</sub>C<sub>6</sub>H<sub>2</sub>, XH = NHTf

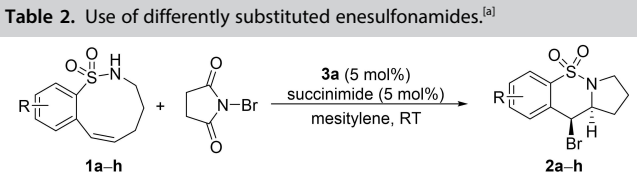
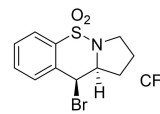
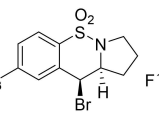
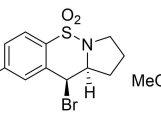
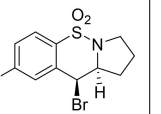
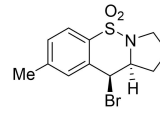
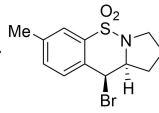
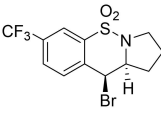
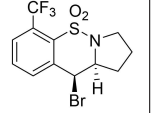


	Cat.	Halogen source	Solvent	Yield [%] <sup>[b]</sup>	<i>ee</i> [%] <sup>[c]</sup>
1	<b>3a</b>	NBS ( <b>4a</b> )	toluene	89	65
2 <sup>[d]</sup>	none	NBS ( <b>4a</b> )	toluene	70	–
3	<b>3b</b>	NBS ( <b>4a</b> )	toluene	92	49
4	<b>3c</b>	NBS ( <b>4a</b> )	toluene	91	40
5	<b>3d</b>	NBS ( <b>4a</b> )	toluene	91	15
6	<b>3e</b>	NBS ( <b>4a</b> )	toluene	89	28
7	<b>3f</b>	NBS ( <b>4a</b> )	toluene	99	17
8	<b>3a</b>	NBS ( <b>4a</b> )	CHCl <sub>3</sub>	91	28
9	<b>3a</b>	NBS ( <b>4a</b> )	PhCl	95	59
10	<b>3a</b>	NBS ( <b>4a</b> )	<i>m</i> -xylene	95	73
11	<b>3a</b>	NBS ( <b>4a</b> )	mesitylene	92	74
12	<b>3a</b>	<b>4b</b>	mesitylene	70	7
13	<b>3a</b>	<b>4c</b>	mesitylene	97	70
14	<b>3a</b>	<b>4d</b>	mesitylene	91	57
15	<b>3a</b>	<b>4e</b>	mesitylene	65	5
16 <sup>[e]</sup>	<b>3a</b>	NBS ( <b>4a</b> )	mesitylene	95	61
17 <sup>[f]</sup>	<b>3a</b>	NBS ( <b>4a</b> )	mesitylene	92	84

[a] Reactions were performed with 0.072 mmol of **1a**, halogenating agent (0.072 mmol), catalyst (5 mol%) and the corresponding solvent (0.5 M) at RT for 15 min. [b] Isolated yield after flash column chromatography purification. [c] Calculated by HPLC on chiral stationary phase (see the Supporting Information). [d] Reaction required for 180 min to reach to full conversion. [e] Reaction carried out at 0 °C for 30 min. [f] 5 mol% of succinimide was incorporated as additive.

out the reaction at lower temperature (0 °C) but this did not result in any significant improvement, only observing a slightly slower reaction (Table 1, entry 16). Finally, the enantioselectivity of the process was increased to 84% *ee* by incorporating 5 mol% of succinimide as additive (Table 1, entry 17), which is supposed to facilitate the proton transfer or activate the halogenating agent in the initial stages of the acid-catalyzed reaction.<sup>[9]</sup> At this point, we also tested the reaction on larger scale achieving the desired aminohalogenated adduct with similar results.<sup>[10]</sup> Moreover, the absolute configuration of the adduct **2a** was established by single-crystal X-ray analysis of an enantiopure sample, for which a monocrystal could be obtained.<sup>[11]</sup>

Once the experimental protocol had been optimized, we next focused on studying the scope and limitations of the reaction to be applied to enesulfonamides incorporating different substituents at the aryl moiety (Table 2).<sup>[12]</sup> As it can be seen in this table, the reaction proceeded with very high yields in all

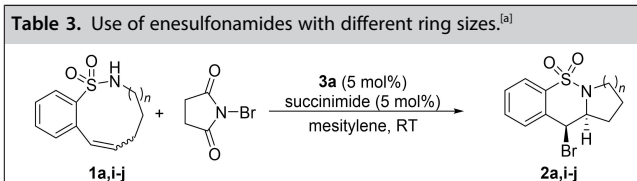
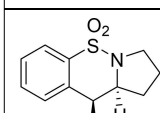
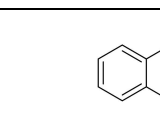
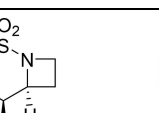
Table 2. Use of differently substituted enesulfonamides. <sup>[a]</sup>	
	
 2a (92%) er 92:8 (15 min)	 2b (80%) er 95:5 (30 min)
 2c (85%) er 82:18 (1 h)	 2d (97%) er 59:41 (15 min)
 2e (92%) er 64:36 (45 min)	 2f (87%) er 80:20 (15 min)
 2g (81%) er 61:39 (2 days)	 2h (67%) <sup>[c]</sup> er 63:37 (22 h)
<p>[a] Reactions were performed with 0.072 mmol of <b>1a–h</b>, NBS (0.072 mmol), succinimide (5 mol%), catalyst <b>3a</b> (5 mol%) in mesitylene (0.5 M) at RT until complete consumption of the starting material (TLC monitoring). Isolated yield after flash column chromatography purification are given and <i>er</i> was calculated by HPLC on chiral stationary phase (see the Supporting Information). [b] Reaction carried out in the absence of succinimide. [c] 18% of the corresponding regioisomer was isolated as well (see the Supporting Information).</p>	

cases regardless the substitution pattern at the substrate. However, the enantioselectivity of the process was strongly affected by both the nature and the position of such substituents. In particular, the reaction performed well when an electron-withdrawing substituent was placed at the *para*-position with respect to the sulfonamide moiety (compounds **2b** and **2c**) but provided very poor enantioselectivity when an electron-donating group was placed at the same position (compounds **2d** and **2e**). The opposite tendency was observed when the substituent was placed at the *meta*-position with respect to the sulfonamide group, obtaining good *er* when an electron-donating group was incorporated (compound **2f**), although the reaction performed much better in the absence of succinimide as additive. In contrast, very poor enantioselectivity was observed when this substituent was replaced by an electron-withdrawing group (compound **2g**). Finally, 2-substituted substrate **1h** also failed to provide the corresponding adduct **2h** with high *er* and, furthermore, in this case the reaction was not completely regioselective, isolating 18% of the isomer.

This observed strong dependence of the enantioselectivity with the substitution pattern was in general attributed to the variable reaction rate of the reaction for each of the substrates tested, which provided an opportunity for the uncatalyzed background reaction to be operative.<sup>[13]</sup> Moreover, it should be highlighted that in the NMR spectra of precursors **1a–h** conformational rigidity could be appreciated, since there are magnetically non-equivalent geminal methylene protons.<sup>[14]</sup>

Taking into account these results, we decided to continue the study by evaluating the effect of modifying the size of the cyclic starting material, concluding that it turns out to be a crucial factor (Table 3). When a smaller ring was used (**1i**), the reaction did not provide the aminobrominating adduct **2i** and when employing substrate **1j** with one more CH<sub>2</sub>, the desired adduct **2j** was isolated in a moderate yield although as a racemic mixture. It should be highlighted that the reaction was completely diastereospecific, observing that **2j** (derived from enesulfonamide **1j** with *E* configuration) presented the protons of the stereogenic centers in a *trans* arrangement.

In view of these results, we turned our attention to evaluate the use of phase-transfer catalysis conditions that, as mentioned, have also provided good results in other reported examples of intramolecular enantioselective aminohalogenation reactions. We started selecting the best halogen source **4f–k** for carrying out the reaction in the presence of the archetypical chiral phosphoric acid (*R*)-TRIP (**3a**) and excess of neat sodium carbonate in mesitylene at room temperature (Table 4, entries 1–6). Under these conditions, the model substrate **1a** was satisfactorily transformed into adduct **2a** regardless the substitution pattern of the halogen source employed, obtaining in all cases the desired product with high yield and promising *ee*. Taking these results into account, together with the difficulty of preparing the halogenating agents, the optimization process was continued with salt **4f** which provided the compound **2a** with 92% yield and 79% *ee* (Table 4, entry 1). Temperature effect was also evaluated (Table 4, entries 7 and 8) and a slight improvement in the enantiocontrol was found working at 0 °C, although longer reaction times were needed in order to reach full conversions (3 h vs. 4.5 h). However, working at lower temperatures (−15 °C) was not beneficial due to the slowing down of the reaction (7 h) and decrease in the yield (Table 4, entry 8). Finally, different solvents mixtures were tested (Table 4, entries 9–11), observing that the model substrate **1a** was converted into transannular aminohalogenation product **2a** in

Table 3. Use of enesulfonamides with different ring sizes. <sup>[a]</sup>	
	
 2a (92%) er 92:8 (15 min)	 2i (<5%) er n.d. <sup>[b]</sup> (30 h)
	 2j (56%) <sup>[c]</sup> er 51:49 (15 min)
<p>[a] Reactions were performed with 0.072 mmol of <b>1a,i–j</b>, NBS (0.072 mmol), succinimide (5 mol%), catalyst <b>3a</b> (5 mol%) in mesitylene (0.5 M) at RT until complete consumption of the starting material (TLC monitoring). Isolated yield after flash column chromatography purification are given and <i>er</i> was calculated by HPLC on chiral stationary phase (see the Supporting Information). [b] n.d.: not determined. [c] The substrate <b>1j</b> was employed as a mixture of <i>E</i>:<i>Z</i> (10:1) diastereoisomers.</p>	

**Table 4.** Optimization of the reaction employing phase-transfer catalysis.<sup>[a]</sup>

**1a**  $\xrightarrow[\text{solvent, 7 } ^\circ\text{C, 3 h}]{\text{halogenating agent 3a (10 mol\%), Na}_2\text{CO}_3 \text{ (1 equiv.)}}$  **2a**

**4f:** R = Cl, X = Cl  
**4g:** R = Cl, X = BF<sub>4</sub>  
**4h:** R = 3,5-(CF<sub>3</sub>)<sub>2</sub>C<sub>6</sub>H<sub>3</sub>, X = Cl  
**4i:** R = 3,5-(CF<sub>3</sub>)<sub>2</sub>C<sub>6</sub>H<sub>3</sub>, X = BF<sub>4</sub>  
**4j:** R = (CH<sub>3</sub>)<sub>5</sub>C<sub>6</sub>, X = Cl  
**4k:** R = (CH<sub>3</sub>)<sub>5</sub>C<sub>6</sub>, X = BF<sub>4</sub>

	Halogen source	Solvent	T [°C]	Yield [%] <sup>[b]</sup>	ee. [%] <sup>[c]</sup>
1	<b>4f</b>	mesitylene	RT	92	79
2	<b>4g</b>	mesitylene	RT	75	78
3	<b>4h</b>	mesitylene	RT	92	78
4	<b>4i</b>	mesitylene	RT	85	79
5	<b>4j</b>	mesitylene	RT	73	75
6	<b>4k</b>	mesitylene	RT	92	80
7	<b>4f</b>	mesitylene	0	86	86
8	<b>4f</b>	mesitylene	-15	45	87
9 <sup>[d]</sup>	<b>4f</b>	mesitylene/hexane (1:1)	0	95	91
10 <sup>[d]</sup>	<b>4f</b>	<i>m</i> -xylene/hexane (1:1)	0	95	87
11 <sup>[d]</sup>	<b>4f</b>	toluene/hexane (1:1)	0	90	84

[a] Reactions were performed with 0.05 mmol of **1a**, brominating agent **4** (0.065 mmol), catalyst **3a** (10 mol%) and Na<sub>2</sub>CO<sub>3</sub> (0.20 mmol) until complete consumption of the starting material (TLC monitoring). [b] Isolated yield after flash column chromatography purification. [c] Calculated by HPLC on chiral stationary phase (see the Supporting Information). [d] Reaction required for 23 h to reach to full conversion.

excellent yield and *ee* after 23 h when a mixture of mesitylene/hexane (1:1) was used (Table 4, entry 9).

After the optimization process, the best conditions involved the use of bromine/ammonium salt adduct **4f** as the most effective halogenating agent in the presence of an excess of neat sodium carbonate, catalyst **3a** and in a binary mesitylene/hexane (1:1) solvent system (Table 4).<sup>[15]</sup> These conditions were subsequently applied to some of the substrates that had previously provided poor stereocontrol in the conditions shown in Table 2. As it can be seen in Table 5, a significant improvement on the enantioselectivity was observed in all cases tested, keeping the excellent yield for all examples.

In order to provide a plausible rationale for the observed reactivity in the Brønsted acid-catalyzed reaction, we decided to study the reaction between **1a** and **2a** catalyzed by **3a** computationally. The conformational flexibility of compound **1a** generates additional issues for the study of the reaction mechanism. Although it is known that nine-membered carbocycles present several conformations of similar energies easily interconverted by pseudorotation,<sup>[16]</sup> the fused aromatic ring, the endocyclic double bond and the sulfonamide group in **1a** introduce nonsymmetric structures and contribute significantly to the ring strain increasing the interconversion barriers. Because of that, it is not possible to carry out a systematic conformational analysis of the sixteen symmetrical configura-

**Table 5.** Enantioselective transannular aminohalogenation under PTC.<sup>[a]</sup>

**1a-h** + **4f**  $\xrightarrow[\text{mesitylene}/n\text{-hexane 1:1, 0 } ^\circ\text{C}]{\text{3a (10 mol\%), Na}_2\text{CO}_3 \text{ (4 equiv.)}}$  **2a-h**

**2a** (95%) *er* 96:4  
**2d** (94%) *er* 84:16  
**2e** (97%) *er* 88:12  
**2g** (95%) *er* 87:13  
**2h** (81%)<sup>[b]</sup> *er* 81:19

[a] Reactions were performed with 0.05 mmol of **1a-h**, brominating agent **4f** (0.065 mmol), catalyst **3a** (10 mol%) and Na<sub>2</sub>CO<sub>3</sub> (0.20 mmol) in a 1:1 mixture of mesitylene and *n*-hexane at 0 °C until complete consumption of the starting material (TLC monitoring). Isolated yields after flash column chromatography purification are given and *er* was calculated by HPLC on chiral stationary phase (see the Supporting Information). [b] 8% of the regioisomer was also isolated (see the Supporting Information).

tions of a nine-membered ring.<sup>[17]</sup> Moreover, the presence of the double bond provides planar chirality to **1a** and constrain the interconversion of enantiomers. To overcome these issues, we performed a conformational analysis of **1a**. A first analysis using molecular dynamics (MD) simulations showed one predominant conformer **A** and small amounts of a second one as the preferred situation at ambient temperature in chloroform as a solvent (Figure 1).

Conformer **A** showed the phenyl group almost perpendicular to the double bond, composing a concave area containing the phenyl group and the three methylenes. All these methylenes are oriented staggered each other and the pyramidalization of the nitrogen pointing out the lone pairs outside the ring.

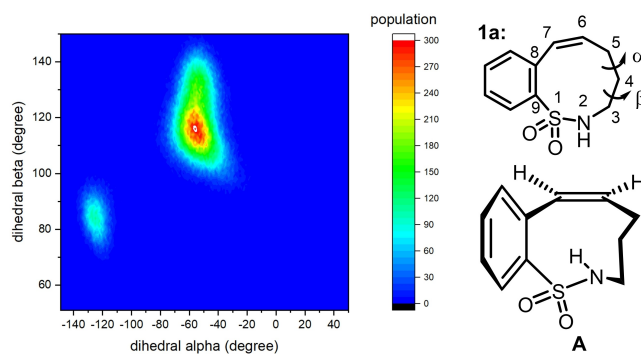


**Figure 1.** Conformational analysis of **1a** by using MD simulations. Population analysis was carried out with 250 000 snapshots. The representation was made on the basis of the more flexible dihedral angles  $\alpha$  and  $\beta$ .

We carried out, in parallel, a conformational search using MacroModel software<sup>[18]</sup> from which we constructed a pseudorotational itinerary of lower energy (for other alternatives and conformations see the Supporting Information; Figure 2). All the transition structures between conformers were located and characterized at wb97xd/def2svp/pcm=toluene level of theory. These transition structures were verified by the corresponding IRC analyses; the corresponding energy profile of optimized points is also given in Figure 2.

The pseudorotational itinerary of **1a** consists of two enantiomeric sections in which conformers **A** and **D**, and the corresponding enantiomers, account for 94 and 6%, respectively, according to a Boltzmann distribution. These results confirmed the MD analysis that predicted the same predominant conformers. The geometrical difference between conformers **A** and **D** resides in the relative orientation of the methylenes. In fact, all the conformers present geometries in which the aromatic ring is out of the plane of the double bond preventing conjugation. Consequently, one enantioface of the double bond points towards the inside region of the molecule (nitrogen atom) and the other one to the outside region. The highest barrier in the conformational itinerary for the interconversion of **A** into *ent*-**A**, is 17.1 kcal mol<sup>-1</sup> and corresponds to the loss of the planar chiral information.<sup>[19]</sup> The kinetic constant calculated for that barrier is 1.78 s<sup>-1</sup> (0.12 s<sup>-1</sup> at 0 °C) and the half-life  $t_{1/2}$  is 0.390 s (6 s at 0 °C). These values agree with a

relatively slow conformational racemization at ambient temperature.

When considering the cyclization reaction, that is, the attack of the nitrogen atom to the activated double bond, conformers **A/D**, and *ent*-**A/ent**-**D** lead to attacks by the 6*Re* and 6*Si* faces of the double bond, respectively. Since a conformational equilibrium connects both enantiomers we could see the whole process as a dynamic kinetic resolution (DKR) when a chiral catalyst is used. According to the Curtin-Hammett principle,<sup>[20]</sup> such a DKR-like scenario would require a faster reaction for one conformer, a slow reaction for the other and a much faster equilibration between them. Consequently, we next studied the cyclization reaction.

Denmark and Burk reported<sup>[9]</sup> that, in the presence of a Lewis base, NBS is cooperatively activated by a phosphoric acid to form a phosphate hypobromite which transfer bromine to the substrate. Accordingly, we can propose the catalytic cycle illustrated in Figure 3. Once formed the reactive halogenating reagent **C1**, an encounter pair **EP** is formed with the reactant (**1a**) leading to a bromiranium intermediate **IN** which evolves to **PR** through **TS2**. Product **PR**, by the action of the Lewis base and NBS, yields the product **2a** and regenerates the active catalytic species **C1**, starting the cycle again. For the calculations, we fixed our attention in the transformation of **EP** into **PR**. Any alternative bifunctional interaction between the catalyst and the sulfonamide group of the substrate can be discarded because it would prevent the *anti*-type intramolecular attack of the nitrogen atom.

We could assume that the reaction takes place with the racemic conformers **A** and *ent*-**A**. However, on the basis of Curtin-Hammett's principle<sup>[20]</sup> the reaction might also take place with racemic **D** and *ent*-**D** which are only 1.7 kcal mol<sup>-1</sup> above the former. Other conformers are too high in energy to be considered as candidates to be the most reactive ones. We carried out the whole study of the process with (*R*)-BINOL-phosphoric acid as a reduced model of the real catalyst. This model, being also chiral, presented a simpler structure which reduces computational cost. Consequently, we approached chiral phosphate hypobromite **C1** to **A**, **D** and their enantiomers by the corresponding enantiotopic faces (6*Si* for **A** and **D**, and 6*Re* for *ent*-**A** and *ent*-**D**). After an exhaustive exploration of the potential energy surface (PES), we located the most stable transition structures corresponding to **TS1a** and **TS1b** formed from **A** and *ent*-**A**, respectively. The IRC's for these transition structures indicated that they connect the corresponding encounter pairs **EPa** and **EPb** with bromiranium intermediates which, after optimization yield **INa** (1.09 kcal mol<sup>-1</sup> lower than **TS1a**) and **INb** (2.1 kcal mol<sup>-1</sup> lower than **TS1b**) as stable stationary points.

It has been reported that in the case of double bonds conjugated with aromatic rings (styrenes and stilbenes), in which there is a quite different electronic distribution due to the substituents, the intermediate formed after bromination features a stabilized carbocation rather than a bromiranium ring.<sup>[21]</sup> An alternate situation between carbocations have also been suggested based on NMR experiments.<sup>[22]</sup> However, as it has been mentioned above, the orientation of the aromatic ring

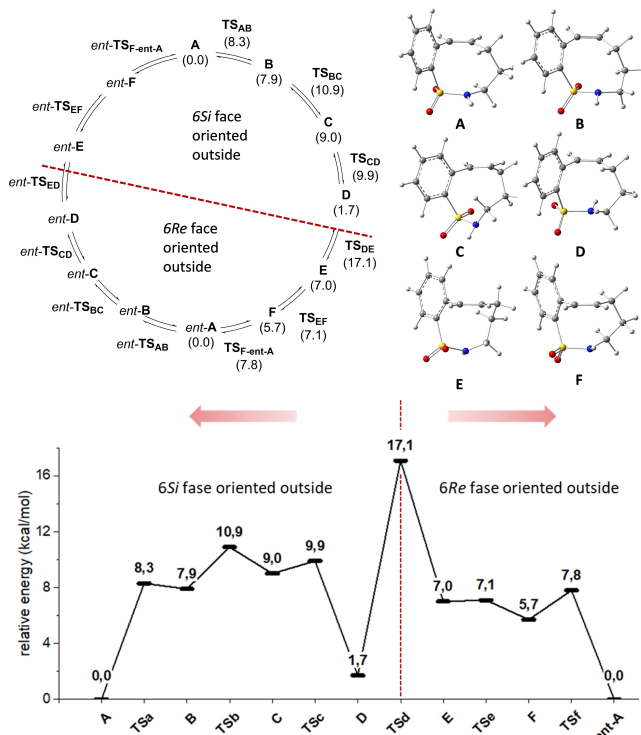


**Figure 2.** Top: Pseudorotational itinerary of lower energy for **1a**. The enantiomeric part is given at the bottom of the catalytic cycle (relative energies [kcal mol<sup>-1</sup>] are given in brackets for one enantiomeric part). Bottom: Energy profile of a half-cycle corresponding to one enantiomeric part.

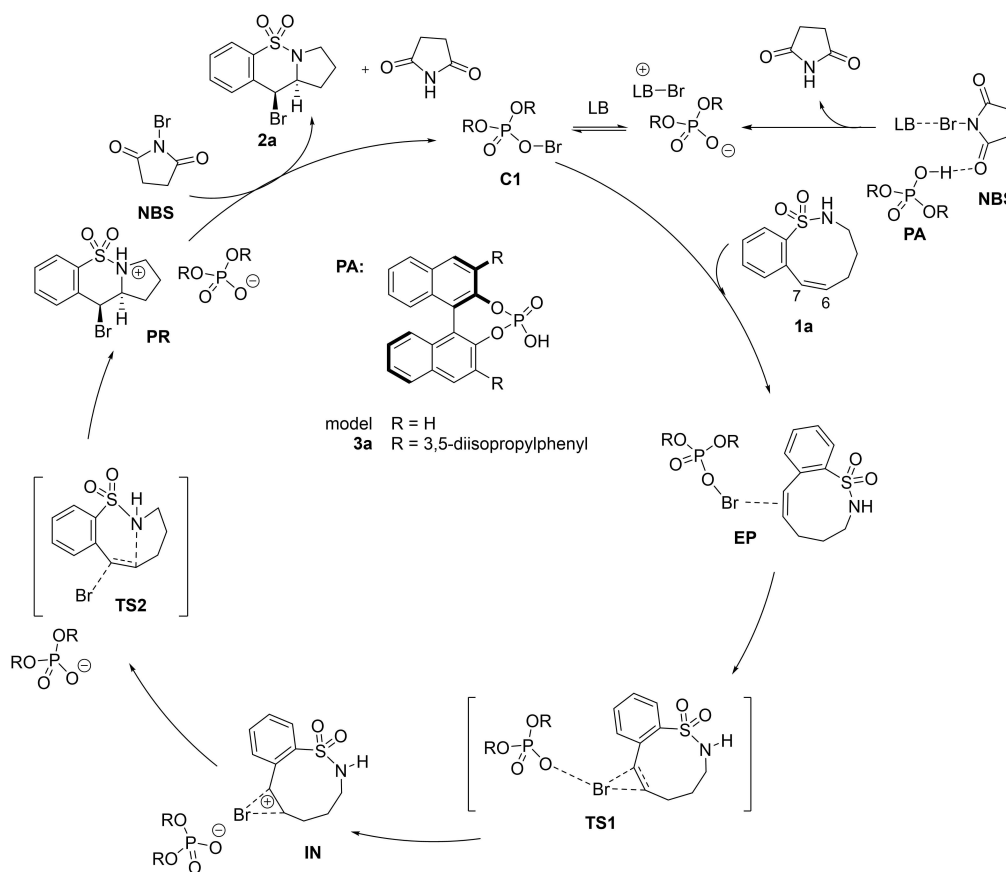


Figure 3. Catalytic cycle for the enantioselective transannular reaction of **1a**.

out of the plane of the double bond prevents conjugation and justifies the absence of a benzylic carbocationic intermediate. In our case, it can be observed for the transition structures that C7 is more pyramidalized than C6, the C7–Br distance (2.39 and 2.40 Å for **TS1a** and **TS1b**, respectively) being shorter than the C6–Br distance (2.51 and 2.52 Å for **TS1a** and **TS1b**, respec-

tively). This is in agreement with the development of an incipient positive charge at homobenzylic position, which, in turn, it should be stabilized by the nitrogen lone pairs. NCI calculations<sup>[23]</sup> corroborated this stabilizing interaction (Figure 4; only the most stable **b** series is showed; for the whole analysis see the Supporting Information). The above situation observed

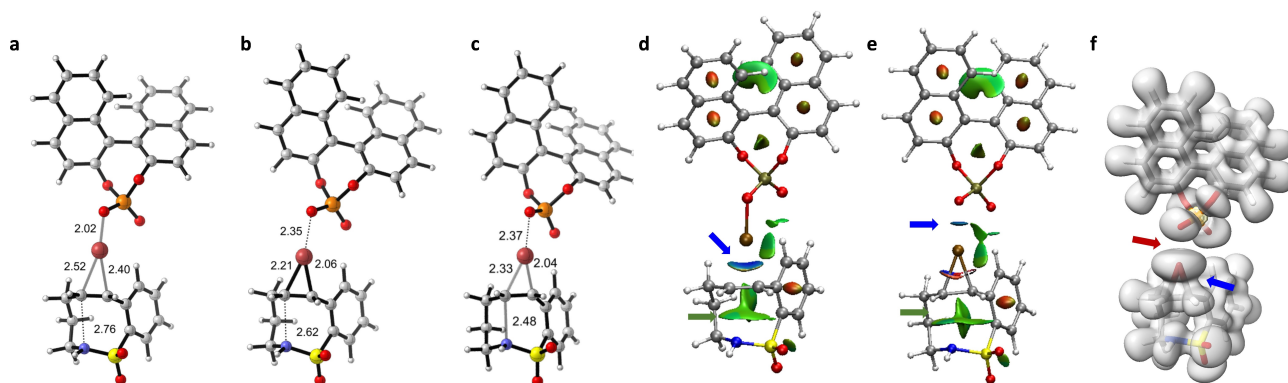


Figure 4. Optimized geometries (wb97xd/def2svp/smd=toluene) of a) **TS1b**, b) **INb** and c) **TS2b**. d) NCI calculations for **TS1b**. The blue arrow indicates a prebonding interaction, and the green arrow points to a stabilizing van der Waals interaction. e) NCI calculations for **INb**. The blue arrow indicates a strong electrostatic interaction, and the green delocalized surface indicates van der Waals interactions. Small, lenticular, bluish surfaces indicate strong interactions. f) ELF of **INb**. The blue arrow indicates the presence of electron density between bromine and carbon atoms. The red arrow confirms the electrostatic interaction by the absence of electron density between bromine and oxygen atoms as expected for an ion-pair.

for **TS1a,b** is maintained in the corresponding intermediates **INa,b** which resulted enough stable to be located and characterized as minima. Again, NCI calculations corroborated the stabilizing interaction of the nitrogen lone pairs. Moreover, the observed distances between P–O and the bromine atom (2.35 Å for both **INa** and **INb**) are more compatible with an electrostatic interaction proper of an ionic pair. Both NCI and ELF<sup>[24]</sup> analyses confirmed the ion-pair character of intermediates, the former revealing a strong electrostatic interaction and the latter demonstrating the absence of electron density between the oxygen and bromine atoms. Those analysis also confirm the nonsymmetric cyclic structure of the bromiranium ring in which the C7...Br distance is shorter than the C6...Br distance as a consequence of a higher partial positive charge of homobenzylic C6. Furthermore, the ELF analysis confirms the presence of some electron density between the bromine atom and both C6 and C7 demonstrating the formation of the three-membered ring.

Bromiranium intermediates **INa,b** evolve through a second transition structure **TS2a,b** to give the products. These transition structures, according to Hammond's postulate<sup>[25]</sup> are rather similar to the precursor intermediates and represent the intramolecular attack of the nitrogen to the homobenzylic position completing the transannular cyclization. The distances in **INa,b** are almost the same that in **TS2a,b** with the exception of the breaking bond C6–Br which is longer in the latter, as expected due to the formation of the C6–N bond.

In terms of energy barriers of the reaction, transition structures **TS1a** and **TS1b** showed barriers with respect to the reagents of 29.4 and 29.0 kcal mol<sup>-1</sup>, and constitute the stereo-differentiating rate-limiting step of the reaction. The formation of the reactive reagent **C1** requires, at least, 23.5 kcal mol<sup>-1</sup> (the energy of the most stable encounter pair **EPa**). This is also compatible with the observed DKR-type process having a barrier of 17.1 kcal mol<sup>-1</sup> for the interconversion of enantiomers (Figure 5). On the other hand, the potential energy surface corresponding to the preferred route (**b** series) is close to flat with a maximum difference between points of 1.9 kcal mol<sup>-1</sup>.

Next, we grew up the model to the real catalyst **3a**. We located the most stable **TS1a-r** and **TS1b-r** after introducing the

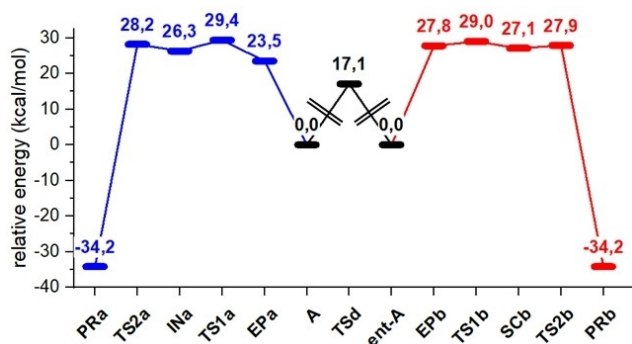


**Figure 5.** Energy profiles (wb97xd/def2tzvp/smd = toluene//wb97xd/def2svp/smd = toluene) for the transformation of **1a** into **PR** catalyzed by BINOL phosphoric acid.

bulky groups into the BINOL system and evaluating the conformational variability of the resulting transition structures. Both transition structures showed barriers referred to starting materials of 23.4 and 24.0 kcal mol<sup>-1</sup> for **TS1a-r** and **TS1b-r**, respectively.

The NCI analysis (see the Supporting Information) reveals stabilizing van der Waals interactions between the catalyst and the substrates that justify the lower barrier calculated for the real model (23.4 vs. 29.0 kcal mol<sup>-1</sup> for the BINOL model). Interactions between the isopropyl groups of the catalyst and the substrate, an aromatic ring in **TS1b-r**, and methylenes in **TS1a-r** are the responsible of the small difference in energy (only 0.6 kcal mol<sup>-1</sup>) observed for the transition structures. This small difference correctly predicts the modest enantiomeric ratio observed experimentally in several cases. The total energy barrier is compatible with the observed interconversion of conformers leading to a DKR-type process. So, these results fully agree with the experimental results featuring a not very enantioselective reaction requiring, in some cases, hours for completion at ambient temperature.

Any attempt of locating a bromiranium intermediate or a second transition structure for the real model failed. Moreover, it was not possible to calculate the IRC of the transition structure due to the flatness of the PES. Because of that, we performed relaxed scans in reverse and forward directions. In all cases downhill pathways were obtained, no minima being present between the corresponding transition structure and the product (**PR**; for details see the Supporting Information). So, it is possible to assume that this part of the reaction—the intramolecular attack of the nitrogen atom to the bromiranium intermediate—is, in this case, almost barrierless.

Calculations of noncovalent interactions of **TS1a,b-r** corroborated the still present interaction between oxygen and bromine atoms as well as that between the nitrogen and the carbon atom at homobenzylic position, confirming that they correspond to the first transition structures. These findings suggest that we are moving through a stepwise process crossing a flat PES in which the second step requires very low energy. The comparison of the observed distances in **TS1a,b** of the BINOL and real models indicates that the bulkiness of the catalyst promotes a transition structure in which the bromine atom approximates the double bond in a more symmetrical way, that is, the C–Br distances are more similar between them than in the BINOL-derived transition structures (C6–Br 2.44 Å and C7–Br 2.45 Å in **TS1b-r** vs. C6–Br 2.52 Å and C7–Br 2.40 Å in **TS1b**). In consonance with such a more symmetrical approach there is a lower stabilization by the nitrogen atom as indicated by a longer C6–N distance in **TS1b-r** (2.81 Å) than for **TS1b** (2.76 Å, Figure 6). Actually, both are stepwise processes but the presence of bulky groups renders more favored a barrierless second step. This situation is substantially different than that reported previously<sup>[26]</sup> in the course of a semi-pinacolinic rearrangement initiated by an alkene halofunctionalization, in which the second part of the reaction took place in a concomitant way with the bromine attack through an only transition structure (Figure 7). The real difference between the two processes is given by the topological NCI and ELF analyses,



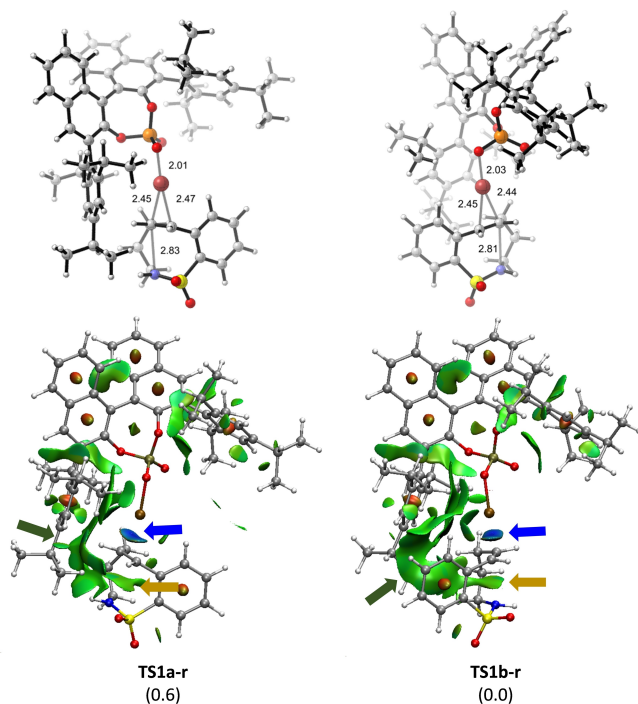


**Figure 6.** Optimized geometries (wb97xd/def2svp/smd = toluene) of the most favored transition structures **TS1a,b-r** for the real catalyst **3a**. Relative energies ( $\Delta\Delta G$ , calculated at wb97xd/def2tzvp/smd = toluene/wb97xd/def2svp/smd = toluene level) are given in brackets in kcal mol<sup>-1</sup>. Bottom: NCI calculations. The blue arrow indicates a prebonding interaction. The ochre arrows indicate stabilizing interactions of the nitrogen atom. The green arrows indicate stabilizing interactions between the catalyst isopropyl group and the aromatic ring of the substrate in **TS1b-r** and the methylenes of the substrate in **TS1a-r**.

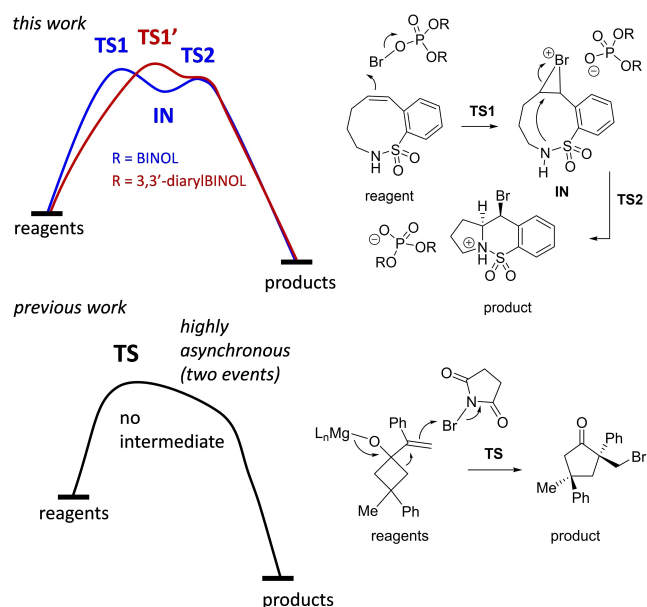


**Figure 7.** Comparison of halofunctionalization of alkenes taking place through stepwise (this work, top) and concerted asynchronous (ref. [26], bottom) mechanisms.

which in the case of the stepwise process described here show an interruption of the electron density when the intermediate is formed. In contrast, in our previously reported halofunctionalization of 1-alkenecyclobutanols, there is a continuous electronic interaction along the whole concerted highly asynchronous reaction.

## Conclusion

In summary, we have shown that chiral phosphoric acids are suitable catalysts for the enantioselective transannular amino-halogenation reaction of enesultams leading to the formation of compounds **2a–h** in excellent yield, diastereoselectivity, and regioselectivity. In order to reach useful enantioselectivities, two complementary methodologies were optimized, one of them based on Brønsted acid catalysis and the other one on PTC. Moreover, enesultam precursors exhibit planar chirality; however, the fast racemization between the most reactive rigid conformers at room temperature allows a DKR process.

Computational studies predict the formation of a bromiranium intermediate with a simple unsubstituted phosphoric acid derived from BINOL. Although the PES is close to planar, with differences of less than 3 kcal mol<sup>-1</sup>, stabilizing interactions of the endocyclic nitrogen atom allow location and characterization as a stationary point, of a nonsymmetrical bromiranium intermediate in which a higher positive charge is partially developed at the homobenzylic position. The absence of conjugation between the aromatic ring and the double bond resulting in planar chirality prevents the formation of a benzylic carbocation. On the other hand, favorable steric van der Waals interactions formed between the substituted BINOL derivative (the real catalyst **3a**) and the substrate causes a decrease in the stabilizing interactions of the nitrogen that promotes the formation of the product through a barrierless second step. The energetics of the process were also predicted correctly as the barrier of the process (availability of the reactive species **C1**) is compatible with the reaction conditions and with the observed equilibration of the reactive conformers (visible by NMR). The small difference between the most favored transition structures for each enantiotopic face is in agreement with the modest values of *ee* observed in several cases. Globally, substitution in the BINOL favored the reaction lowering the energy barrier by 5–6 kcal mol<sup>-1</sup> with respect to the unsubstituted derivative.

## Experimental Section

**Synthesis of 2a, using Brønsted acid catalysis:** A reaction vial was equipped with a magnetic stirring bar, and charged with the substrate **1a** (16.1 mg, 0.072 mmol) and succinimide (0.4 mg, 0.0036 mmol). To the mixture, under argon atmosphere, a solution of (*R*)-TRIP hydrogen phosphate (**3a**; 2.7 mg, 0.0036 mmol) was added, followed by dry mesitylene (0.15 mL). After thermostating the mixture at 25 °C, *N*-bromosuccinimide (12.8 mg, 0.072 mmol) was added. When the reaction was judged complete (15 min), a saturated aqueous solution of NaHCO<sub>3</sub> (1 mL) was added and the mixture was extracted with CH<sub>2</sub>Cl<sub>2</sub> (3 × 10 mL). The combined organic layers were dried over Na<sub>2</sub>SO<sub>4</sub>, filtered and concentrated in

vacuo. Purification of the crude by flash column chromatography on silica gel (petroleum ether/EtOAc, 7:3) gave the corresponding product **2a** (20.0 mg, 92%) as a white solid.  $[\alpha]_D^{20} = +49.2$  ( $c = 1.0$ ,  $\text{CH}_2\text{Cl}_2$ ); The *er* was determined by HPLC using a Chiralpak AS-H column [*n*-hexane/*i*PrOH (70:30)]; flow rate  $1.0 \text{ mL min}^{-1}$ ;  $\tau_1 = 22.0 \text{ min}$ ,  $\tau_2 = 53.2 \text{ min}$  (92:8 *er*).

**Synthesis of 2a, using phase-transfer catalysis:** A reaction vial was equipped with a magnetic stirring bar, and charged with the substrate **1a** (11.2 mg, 0.05 mmol),  $\text{Na}_2\text{CO}_3$  (21.2 mg, 0.2 mmol) and (*R*)-TRIP hydrogen phosphate (**3a**; 3.8 mg, 0.005 mmol). To this vial, under argon atmosphere, 0.5 mL of dry mesitylene and 0.5 mL of dry hexane were added. After thermostating the mixture at  $0^\circ\text{C}$ , the cationic brominating reagent (**4f**; 23.2 mg, 0.065 mmol) was added. When the reaction was judged complete monitored by TLC (48 h), a saturated aqueous solution of  $\text{Na}_2\text{S}_2\text{O}_3$  (1 mL) was added and, after disappearance of the yellow color, the mixture was extracted with  $\text{CH}_2\text{Cl}_2$  ( $3 \times 10 \text{ mL}$ ). The combined organic layers were dried over  $\text{Na}_2\text{SO}_4$ , filtered and concentrated in vacuo. Purification of the crude by column chromatography on silica gel gave the corresponding product **2a** (14.8 mg, 98%) as a white solid.  $[\alpha]_D^{20} = +50.7$  ( $c = 1.0$ ,  $\text{CH}_2\text{Cl}_2$ ); The *er* was determined by HPLC using a Chiralpak OD-3 column [*n*-hexane/*i*PrOH (70:30)]; flow rate  $1.0 \text{ mL min}^{-1}$ ;  $\tau_1 = 8.7 \text{ min}$ ,  $\tau_2 = 14.6 \text{ min}$  (96:4 *er*).

**Spectral data of compound 2a:** m.p. (petroleum ether/EtOAc):  $145\text{--}148^\circ\text{C}$ ;  $^1\text{H NMR}$  (300 MHz,  $\text{CDCl}_3$ ):  $\delta = 7.88$  (dd,  $J = 7.5$ , 1.0 Hz, 1H,  $\text{C}_{\text{arom}}\text{-H}$ ), 7.62–7.46 (m, 3H,  $\text{C}_{\text{arom}}\text{-H}$ ), 5.51 (d,  $J = 3.3$  Hz, 1H,  $\text{C}_{10}\text{-H}$ ), 4.12 (ddd,  $J = 7.6$ , 6.3, 3.3 Hz, 1H,  $\text{C}_{10\text{a}}\text{-H}$ ), 3.63 (ddd,  $J = 9.1$ , 6.7, 5.1 Hz, 1H,  $\text{C}_3\text{-H}_\text{a}\text{H}_\text{b}$ ), 3.53–3.32 (m, 1H,  $\text{C}_3\text{-H}_\text{a}\text{H}_\text{b}$ ), 2.42–2.19 (m, 1H,  $\text{C}_1\text{-H}_\text{a}\text{H}_\text{b}$ ), 2.19–1.88 (m, 3H,  $\text{C}_1\text{-H}_\text{a}\text{H}_\text{b}$ ,  $\text{C}_2\text{-H}$ );  $^{13}\text{C NMR}$  (75 MHz,  $\text{CDCl}_3$ ):  $\delta = 136.8$  ( $\text{C}_{\text{arom}}\text{-S}$ ), 135.2 ( $\text{C}_{\text{arom}}\text{-C}_{10}$ ), 132.7 ( $\text{C}_{\text{arom}}\text{-H}$ ), 130.6 ( $\text{C}_{\text{arom}}\text{-H}$ ), 129.7 ( $\text{C}_{\text{arom}}\text{-H}$ ), 124.4 ( $\text{C}_{\text{arom}}\text{-H}$ ), 62.1 ( $\text{C}_{10\text{a}}$ ), 50.7 ( $\text{C}_{10}$ ), 46.7 ( $\text{C}_3$ ), 31.5 ( $\text{C}_1$ ), 23.7 ( $\text{C}_2$ ); IR (ATR): 1303 ( $\text{SO}_2$  st as), 1260 ( $\text{C-N}$  st),  $1155 \text{ cm}^{-1}$  ( $\text{SO}_2$  st sym); MS (EI) *m/z* (%): 221 ( $[\text{M-HBr}]^+$ , 97), 156 (100), 130 (19), 129 (33), 128 (30), 115 (20), 102 (19), 89 (20), 63 (20); HRMS (UPLC MS  $\text{ESI}^+$ ): Calculated for  $[\text{C}_{11}\text{H}_{13}\text{NO}_2\text{SBr}]^+$ : 301.9845 [ $\text{M} + \text{H}]^+$ ; found: 301.9848.

## Acknowledgements

The authors thank the Spanish Ministerio de Ciencia, Innovación y Universidades (FEDER PID2020-118422GB-I00 and FEDER PID2019-104090RB-I00), the Basque Government (Grupos IT1558-22 and postdoctoral contract to J.L.-B.) and the Regional Government of Aragon (Grupos 17R-34) for financial support. Predoctoral FPU fellowship to S.R. from the Spanish Ministry of Education and to M.P. from Government of Aragon are also acknowledged. The authors thankfully acknowledge the resources from the super-computers “Memento” and “Cierzo”, technical expertise and assistance provided by BIFI-ZCAM (Universidad de Zaragoza, Spain).

## Conflict of Interest

The authors declare no conflict of interest.

## Data Availability Statement

The data that support the findings of this study are available on request from the corresponding author. The data are not publicly available due to privacy or ethical restrictions.

**Keywords:** asymmetric catalysis · computational chemistry · electrophilic addition · ELF · medium-ring compounds · transannular reactions

- [1] For some reviews, see: a) E. Marsault, A. Toro, P. Nowak, P. Deslongchamps, *Tetrahedron* **2001**, *57*, 4243–4260; b) S. Handa, G. Pattenden, *Contemp. Org. Synth.* **1997**, *4*, 196–215; c) A. M. Montana, C. Batalla, J. A. Barcia, *Curr. Org. Chem.* **2009**, *13*, 919–938; d) A. Rizzo, S. R. Harutyunyan, *Org. Biomol. Chem.* **2014**, *12*, 6570–6579; e) E. Reyes, U. Uria, L. Carrillo, J. L. Vicario, *Tetrahedron* **2014**, *70*, 9461–9484; f) P. A. Clarke, A. T. Reeder, J. Winn, *Synthesis* **2009**, *5*, 691–709.
- [2] For some selected recent examples, see: a) K. Takao, H. Kai, A. Yamada, Y. Fukushima, D. Komatsu, A. Ogura, K. Yoshida, *Angew. Chem. Int. Ed.* **2019**, *58*, 9851–9855; *Angew. Chem.* **2019**, *131*, 9956–9960; b) X. Liu, J. Liu, J. Wu, G. Huang, R. L. Liang, W. Chung, C.-C. Li, *J. Am. Chem. Soc.* **2019**, *141*, 2872–2877; c) B. Maiga-Wandiam, A. Corbu, G. Massiot, F. Sautel, P. Yu, B. W.-Y. Lin, K. N. Houk, J. Cossy, *J. Org. Chem.* **2018**, *83*, 5975–5985; d) C. Leitner, T. Gaich, *Chem. Commun.* **2017**, *53*, 7451–7453; e) T. Kang, K. L. White, T. J. Mann, A. H. Hoveyda, M. Movassaghi, *Angew. Chem. Int. Ed.* **2017**, *56*, 13857–13860; *Angew. Chem.* **2017**, *129*, 14045–14048; f) M. Ohtawa, M. J. Krambis, R. Cerne, J. M. Schkeryantz, J. M. Witkin, R. A. Shenvi, *J. Am. Chem. Soc.* **2017**, *139*, 9637–9644; g) A. Minassi, F. Pollastro, G. Chianese, D. Caprioglio, O. Tagliatalata-Scafati, G. Appendino, *Angew. Chem. Int. Ed.* **2017**, *56*, 7935–7938; *Angew. Chem.* **2017**, *129*, 8043–8046; h) D. Dagonneau, Z. Xu, Q. Wang, J. Zhu, *Angew. Chem. Int. Ed.* **2016**, *55*, 760–763; *Angew. Chem.* **2016**, *128*, 770–773; i) H. Umihara, T. Yoshino, J. Shimokawa, M. Kitamura, T. Fukuyama, *Angew. Chem. Int. Ed.* **2016**, *55*, 6915–6918; *Angew. Chem.* **2016**, *128*, 7029–7032; j) K. C. Nicolaou, A. A. Shah, H. Korman, T. Khan, L. Shi, W. Worawalai, E. A. Theodorakis, *Angew. Chem. Int. Ed.* **2015**, *54*, 9203–9208; *Angew. Chem.* **2015**, *127*, 9335–9340; k) P. Yu, A. Patel, K. N. Houk, *J. Am. Chem. Soc.* **2015**, *137*, 13518–13523; l) C. Zhu, Z. Liu, G. Chen, K. Zhang, H. Ding, *Angew. Chem. Int. Ed.* **2015**, *54*, 879–882; *Angew. Chem.* **2015**, *127*, 893–896; m) J. Han, F. Li, C. Li, *J. Am. Chem. Soc.* **2014**, *136*, 13610–13613; n) A. S. Lee, B. B. Liau, M. D. Shair, *J. Am. Chem. Soc.* **2014**, *136*, 13442–13452.
- [3] a) O. Knopff, J. Kuhne, C. Fehr, *Angew. Chem. Int. Ed.* **2007**, *46*, 1307–1310; *Angew. Chem.* **2007**, *119*, 1329–1332; b) A. Dermenci, P. S. Selig, R. A. Domaol, K. A. Spasov, K. S. Anderson, S. J. Miller *Chem. Sci.* **2011**, *2*, 1568–1572; c) E. P. Balskus, E. N. Jacobsen, *Science* **2007**, *317*, 1736; d) N. S. Rajapaksa, E. N. Jacobsen, *Org. Lett.* **2013**, *15*, 4238–4241; e) T. Jaschinski, M. Hiersemann, *Org. Lett.* **2012**, *14*, 4114–4117; f) C. L. Chandler, B. List, *J. Am. Chem. Soc.* **2008**, *130*, 6737–6739; g) R. Mato, R. Manzano, E. Reyes, L. Carrillo, U. Uria, J. L. Vicario *J. Am. Chem. Soc.* **2019**, *141*, 9495–9499; h) R. Mato, E. Reyes, L. Carrillo, U. Uria, L. Prieto, R. Manzano, J. L. Vicario *Chem. Commun.* **2020**, *56*, 13149–13152; i) J. Sendra, R. Manzano, E. Reyes, J. L. Vicario, E. Fernández *Angew. Chem. Int. Ed.* **2020**, *59*, 2100–2104; *Angew. Chem.* **2020**, *132*, 2116–2120.
- [4] For some selected examples: a) N. D. P. Atmuri, D. J. Reilly, W. D. Lubell, *Org. Lett.* **2017**, *19*, 5066–5069; b) E. A. Brock, S. G. Davies, J. A. Lee, P. M. Roberts, J. E. Thomson, *Org. Biomol. Chem.* **2013**, *11*, 3187–3202; c) M. Cakmak, P. Mayer, D. Trauner, *Nat. Chem.* **2011**, *3*, 543–545; d) N. D. P. Atmuri, W. D. Lubell, *J. Org. Chem.* **2020**, *85*, 1340–1351; e) A. Sudau, W. Münch, J.-W. Bats, U. Nubbemeyer, *Chem. Eur. J.* **2001**, *7*, 611–621; f) M. Diederich, U. Nubbemeyer, *Chem. Eur. J.* **1996**, *2*, 894–900; g) M. K. Boukanoun, X. Hou, L. Nikolajev, S. Ratni, D. Olson, A. Claing, S. A. Laporte, S. Chemtob, W. D. Lubell, *Org. Biomol. Chem.* **2015**, *13*, 7750–7761.
- [5] For some reviews on enantioselective halofunctionalization, see: a) Y. Cai, X. Liu, Xiaohua, P. Zhou, X. Feng, Xiaoming *J. Org. Chem.* **2019**, *84*, 1–13; b) B. S. Moore *Synlett* **2018**, *29*, 401–409; c) G. Chen, S. Ma, *Angew. Chem. Int. Ed.* **2010**, *49*, 8306–8308; *Angew. Chem.* **2010**, *122*, 8484–8486; d) A. J. Cresswell, S. T.-C. Eey, S. E. Denmark, *Angew. Chem. Int. Ed.* **2015**, *54*, 15642–15682; *Angew. Chem.* **2015**, *127*, 15866–15909; e) Y. A. Cheng, W. Z. Yu, Y.-Y. Yeung, *Org. Biomol. Chem.* **2014**, *12*, 2333–2343;

- f) S. E. Denmark, W. E. Kuester, M. T. Burk, T. Matthew, *Angew. Chem. Int. Ed.* **2012**, *51*, 10938–10953; *Angew. Chem.* **2012**, *124*, 11098–11113; g) S. Zheng, C. M. Schienebeck, W. Zhang, H.-Y. Wang, W. Tang, *Asian J. Org. Chem.* **2014**, *3*, 366–376; h) H. D. Khanal, R. S. Thombal, S. M. B. Maezono, Y. R. Lee, *Adv. Synth. Catal.* **2018**, *360*, 3185–3212.
- [6] a) C. Lebé, F. Blanchard, G. Masson, *Synlett* **2016**, *27*, 559–563; b) A. Alix, C. Lalli, P. Retailleau, G. Masson, *J. Am. Chem. Soc.* **2012**, *134*, 10389–10392; c) D. Huang, H. Wang, F. Xue, H. Guan, L. Li, X. Peng, Y. Shi, *Org. Lett.* **2011**, *13*, 6350–6353; d) Y. Lu, H. Nakatsuji, Y. Okumura, L. Yao, K. Ishihara, *J. Am. Chem. Soc.* **2018**, *140*, 6039–6043; e) H. Nakatsuji, Y. Sawamura, A. Sakakura, K. Ishihara, *Angew. Chem. Int. Ed.* **2014**, *53*, 6974–6977; *Angew. Chem.* **2014**, *126*, 7094–7097; f) R. C. Samanta, H. Yamamoto, *J. Am. Chem. Soc.* **2017**, *139*, 1460–1463; g) S. E. Denmark, M. T. Burk, *Chirality* **2014**, *26*, 356–360.
- [7] a) W. Xie, G. Jiang, H. Liu, J. Hu, X. Pan, H. Zhang, X. Wan, Y. Lai, D. Ma, *Angew. Chem. Int. Ed.* **2013**, *52*, 12924–12927; *Angew. Chem.* **2013**, *125*, 13162–13165; b) Y.-M. Wang, J. Wu, C. Hoong, V. Rauniyar, F. D. Toste, *J. Am. Chem. Soc.* **2012**, *134*, 12928–12931; c) Z. Xia, J. Hu, Z. Shen, X. Wan, Q. Yao, Y. Lai, J.-M. Gao, W. Xie, *Org. Lett.* **2016**, *18*, 80–83; d) E. Miller, S. Kim, K. Gibson, J. S. Derrick, F. D. Toste, *J. Am. Chem. Soc.* **2020**, *142*, 8946–8952; e) H.-J. Long, Y.-L. Li, B.-Q. Zhang, W.-Y. Xiao, X.-Y. Zhang, L. He, *Org. Lett.* **2021**, *23*, 8153–8157; f) H. Xiong, K. Yoshida, K. Okada, H. Ueda, H. Tokuyama, *Tetrahedron Lett.* **2022**, DOI:10.1016/j.tetlet.2022.153906.
- [8] Other halogenating reagents such as NCS and NIS failed to provide the corresponding adducts with good results. For a more detailed screening of halogenating agents, see the Supporting Information.
- [9] S. E. Denmark, M. T. Burk, *Org. Lett.* **2012**, *14*, 256–259.
- [10] When the reaction was carried out using 1 mmol of **1a**, compound **2a** was isolated in 90% yield and 82% ee (see the Supporting Information for details).
- [11] Deposition Number 2189729 (for **2a**) contains the supplementary crystallographic data for this paper. These data are provided free of charge by the joint Cambridge Crystallographic Data Centre and Fachinformationszentrum Karlsruhe Access Structures service.
- [12] The configuration of all other adducts (**2b-h**) was established by assuming the same stereochemical outcome for all reactions based on mechanistic analogy.
- [13] The temperature effect was investigated for substrate **1e** trying to improve the enantioselectivity of the process by decreasing the background reaction, however, working at 0°C did not improve the results previously obtained (61% yield and 22% ee).
- [14] For more details about the conformational rigidity of the substrate **1a**, see computational studies and Supporting Information.
- [15] When the reaction was carried out in 1 mmol scale similar results were obtained (see the Supporting Information for details).
- [16] a) M. Saunders, *J. Comput. Chem.* **1991**, *12*, 645–663; b) K. B. Wiberg, *J. Org. Chem.* **2003**, *68*, 9322–9329.
- [17] M. Randic, *Int. J. Quantum Chem.* **1995**, *22*, 61–73.
- [18] MacroModel, Schrödinger, LLC, New York, NY, 2022–1.
- [19] While conformers **A**, **B**, **C**, **D**, *ent-E* and *ent-F* present the 6*Re* face towards the nitrogen atom, compounds **E**, **F**, *ent-A*, *ent-B*, *ent-C* and *ent-D* present the 6*Si* face towards the nitrogen atom. **TSd** corresponds to the exchange of the orientation of the enantiofaces of the double bond.
- [20] J. I. Seeman, *Chem. Rev.* **1983**, *83*, 83–134.
- [21] a) H. Haubenstock, R. R. Sauers, *Tetrahedron* **2005**, *61*, 8358–8365; b) L. J. McAllister, D. W. Bruce, P. B. Karadakov, *Phys. Chem. Chem. Phys.* **2014**, *16*, 2576–2587.
- [22] B. K. Ohta, R. E. Hough, J. W. Schubert, *Org. Lett.* **2007**, *9*, 2317–2320.
- [23] a) E. R. Johnson, S. Keinan, P. Mori-Sanchez, J. Contreras-Garcia, A. J. Cohen, W. Yang, *J. Am. Chem. Soc.* **2010**, *132*, 6498–6506; b) R. A. Boto, F. Peccati, R. Laplaza, C. Quan, A. Carbone, J.-P. Piquemal, Y. Maday, J. Contreras-Garcia, *J. Chem. Theory Comput.* **2020**, *16*, 4150–4158.
- [24] The electron localization function (ELF) was introduced by Becke and Edgecombe as a “simple measure of electron localization in atomic and molecular systems”. See: a) A. D. Becke, K. E. Edgecombe, *J. Chem. Phys.* **1990**, *92*, 5397–5403; b) Y. Grin, A. Savin, B. Silvi in *The Chemical Bond: Fundamental Aspects of Chemical Bonding* (Eds.: G. Frenking, S. Shaik), Wiley-VCH, Weinheim, **2014**, pp. 345–382.
- [25] G. S. Hammond, *J. Am. Chem. Soc.* **1955**, *77*, 334–338.
- [26] E. Capel, M. Rodriguez-Rodriguez, U. Uriá, M. Pedron, T. Tejero, J. L. Vicario, P. Merino, *J. Org. Chem.* **2022**, *87*, 693–707.

---

Manuscript received: July 19, 2022

Accepted manuscript online: September 16, 2022

Version of record online: October 17, 2022